Weierstraß-Institut
für Angewandte Analysis und Stochastik

im Forschungsverbund Berlin e.V.

Simulation of Microwave and Semiconductor Laser Structures Including Absorbing Boundary Conditions

Georg Hebermehl[1], Friedrich-Karl Hübner[1], Rainer Schlundt[1],

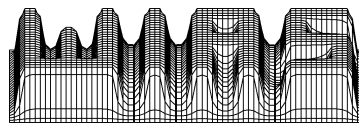Thorsten Tischler[2], Horst Zscheile[2], Wolfgang Heinrich[2]

[1] Weierstrass-Institute for
    Applied Analysis and Stochastics,
    Mohrenstraße 39
    D - 10117 Berlin
    Germany
    E-Mail: hebermehl@wias-berlin.de,
    huebner@wias-berlin.de,
    schlundt@wias-berlin.de

[2] Ferdinand-Braun-Institut für
    Höchstfrequenztechnik,
    Albert-Einstein-Str. 11
    D - 12489 Berlin
    Germany
    E-Mail: tischler@fbh-berlin.de,
    zscheile@fbh-berlin.de,
    w.heinrich@ieee.org

Abstract

The transmission properties of microwave and optical structures can be described in terms of their scattering matrix using a three-dimensional boundary value problem for Maxwell's equations. The computational domain is truncated by electric or magnetic walls, open structures are treated using the Perfectly Matched Layer (PML) Absorbing Boundary Condition. The boundary value problem is solved by a finite-volume scheme. This results in a two-step procedure: an eigenvalue problem for general complex matrices and the solution of a large-scale system of linear equations with indefinite symmetric complex matrices. The modes of smallest attenuation are located in a longsome region bounded by two parabolas, and are found solving a sequence of eigenvalue problems of modified matrices. To reduce the execution times a coarse and a fine grid, and two levels of parallelization can be used. For the computation of the discrete grid equations, advanced preconditioning techniques are applied to reduce the dimension and the number of iterations solving the large-scale systems of linear algebraic equations. These matrix problems need to be solved repeatedly for different right-hand sides, but with the same coefficient matrix. The used block quasi-minimal residual algorithm is a block Krylov subspace iterative method that incorporates deflation to delete linearly and almost linearly dependent vectors in the block Krylov sequences. Special attention is paid to the PML which causes significantly increased number of iterations within Krylov subspace methods.

Contents

List of Figures

1 Introduction

The fields of applications include mobile communications, radio links, automobile radar systems, optical communications, and material processing. The commercial applications of microwave circuits cover the frequency range between 1 GHz and about 100 GHz; special applications in radioastronomy use even higher frequencies up to 1 THz. For optoelectronic devices frequencies about several hundred THz are common.

The subject under investigation are passive structures of arbitrary geometry. They are connected to the remaining circuit by transmission lines. Ports p (see Fig. 1) are defined on the transmission lines outer terminations. In order to characterize their electrical behavior the transmission lines are assumed to be infinitely long and longitudinally homogeneous. Short parts of the transmission lines and the passive structure form the so-called discontinuity. This structure has to be surrounded with an enclosure.
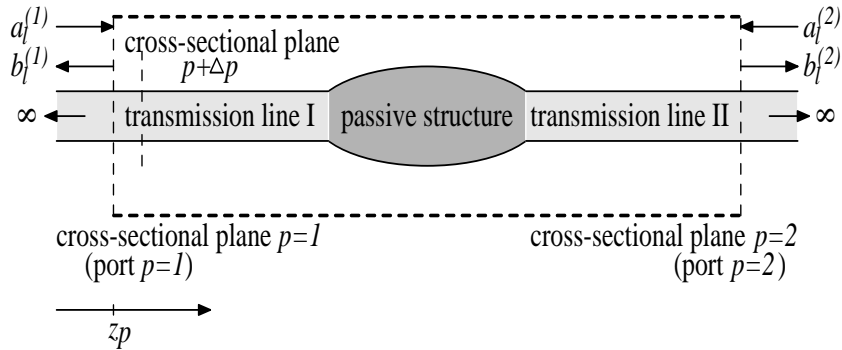
Figure 1: Structure under investigation

The scattering matrix describes the structure in terms of wave modes on the transmission line sections at the ports. One can extract this matrix from the orthogonal decomposition of the electric field at two neighboring cross-sectional planes on each transmission line for a number of linearly independent excitations.

A three-dimensional boundary value problem can be formulated using the integral form of Maxwell's equations in the frequency domain in order to compute the electromagnetic field [1] and subsequently the scattering matrix. For numerical treatment, the computational domain has to be truncated by electric or magnetic walls or by a so-called Absorbing Boundary Condition (ABC) simulating open space. Among the ABC's, the Perfectly Matched Layer (PML) [12] technique represents the most powerful formulation. At the ports the transverse electric field is given by superposing transmission line modes. The transverse electric mode fields are the solutions of an eigenvalue problem for the transmission lines [2].

Maxwell's equations are discretized with staggered nonequidistant rectangular grids, using the Finite Integration Technique (FIT) [19], [1], [7], that transforms the continuous Maxwell equations into a set of discrete Maxwellian grid equations.

Assuming longitudinal homogeneity for the transmission line structure gives an eigenvalue problem for the computation of the transverse electric mode fields.

Only a few modes of smallest attenuation are able to propagate and have to be taken into consideration. Using a conformal mapping between the plane of propagation constants and the plane of eigenvalues the task is to compute all eigenmodes in a region, bounded by two parabolas. The region is covered by a number of overlapping circles. The eigenmodes in these circles are found solving a sequence of eigenvalue problems of modified matrices with the aid of the invert mode of the Arnoldi iteration [10], [16] using shifts.

The PML influences the mode spectrum. Modes that are related to the PML boundary can be detected, using the power part criterion given with [18].

The integral over the power density vector, required for the calculation of the scatter-

ing matrix, of the power part criterion, and for the orthogonalization of eigenvectors, is computed for the used staggered grids.

In the case of multiple eigenvalues the eigenfunctions are orthogonalized according to the orthogonality relation for the scattering matrix using the algorithm of Gram-Schmidt [17].

The presented method, developed initially for a reliable calculation of all complex eigenvalues from microwave structure computations [9], is expanded to meet the very special requirements of optoelectronic structure calculations. Relatively large cross sections and highest frequencies yield increased dimensions and numbers of eigenvalue problems. Using the results of a coarse grid calculation within the final fine grid calculation yields a remarkable reduced numerical effort. The use of two levels of parallelization results in an additional speed up of computation time.

After solution of the eigenvalue problem all boundary conditions are known and we can solve the boundary value problem to compute the three-dimensional electric field. The electromagnetic fields are calculated by the solution of large-scale systems of linear equations with indefinite complex symmetric coefficient matrices. In general, these matrix problems have to be solved repeatedly for different right-hand sides, but with the same coefficient matrix. The number of right-hand sides depends on the number of ports and modes. The systems of linear equations are solved using a block Krylov subspace iterative method. Independent set orderings, Jacobi and SSOR preconditioning techniques are applied to reduce the dimension and the number of iterations [15]. In comparison to the simple lossy case the number of iterations of Krylov subspace methods increases significantly in the presence of Perfectly Matched Layers. This growth is reduced by applying suitable grids and PML properties. This criterion is based on the comparison between the power concentration inside the PML region to the whole computational domain.

In general, the computation of the eigenvalue problem and of the system of linear algebraic equations have to be done for several frequencies.

2   Scattering Matrix

The scattering matrix

$$
S = \begin{pmatrix} S_{11} & S_{12} & \cdots & S_{1m_s} \\ S_{21} & S_{22} & \cdots & S_{2m_s} \\ \cdots\cdots\cdots\cdots\cdots\cdots\cdots \\ S_{m_s 1} & S_{m_s 2} & \cdots & S_{m_s m_s} \end{pmatrix} = (S_{\rho,\sigma}), \quad \rho,\sigma = 1(1)m_s, \tag{1}
$$

$$
\text{with} \quad m_s = \sum_{p=1}^{\overline{p}} m^{(p)}, \quad \rho = l + \sum_{q=1}^{p-1} m^{(q)}, \tag{2}
$$

4

describes the energy exchange and phase relation between all outgoing and all incoming modes. $m^{(p)}$ denotes the number of modes which have to be taken into account at the port p. $\bar{p}$ is the number of ports. The modes on a port p are numbered with l. To simplify matters, the cross-sectional planes and ports coincide in the structure under investigation (see Fig. 1). Generally, more than one port can be defined on one cross-sectional plane.

The scattering matrix can be extracted from the orthogonal decomposition of the electric field (see (3)) at a pair of neighboring cross-sectional planes z_p and $z_{p+\Delta p}$ (see Fig. 1) on each waveguide for a number of linear independent excitations of the transmission lines. The electric fields at the cross-sectional planes z_p and $z_{p+\Delta p}$ are the solutions of an eigenvalue (see section 5) and of a boundary value problem (see section 3), respectively.

The transverse electric mode fields $\vec{E}_{t,l}(z)$ satisfy an orthogonality relation

$$\int_{\Omega} (\vec{E}_{t,l}(z) \times \vec{H}_{t,m}(z)) \cdot d\vec{\Omega} = \eta_m \delta_{l,m}. \tag{3}$$

Here $\vec{H}_{t,m}$ are the transverse magnetic mode fields.

In the case of degenerate modes, i.e., the algebraic multiplicity of the corresponding eigenvalues is greater than 1, we have to use first (3) in order to orthogonalize the modes (see section 9).

We consider all exciting modes with amplitudes a_l in positive z-direction and all outgoing modes with amplitudes b_l in negative z-direction. The transverse mode field at a cross-sectional plane z is given by

$$\vec{E}_t(z) = \sum_{l=1}^{m^{(p)}} a_l \vec{E}_{t,l} e^{-\jmath k_{z_l} z} + \sum_{l=1}^{m^{(p)}} b_l \vec{E}_{t,l} e^{+\jmath k_{z_l} z} = \sum_{l=1}^{m^{(p)}} w_l(z) \vec{E}_{t,l} \tag{4}$$

with

$$w_l(z) = a_l e^{-\jmath k_{z_l} z} + b_l e^{+\jmath k_{z_l} z} = \tilde{a}_l(z) + \tilde{b}_l(z), \tag{5}$$

where k_{z_l} is the propagation constant. The application of (4) with (5) at a pair of two neighboring cross-sectional planes z_p and $z_{p+\Delta p}$ gives because of $\vec{H}_{t,m}^{(p+\Delta p)} = \vec{H}_{t,m}^{(p)}$:

$$
\begin{array}{lllll}
\frac{1}{\eta_m} \int_{\Omega} (\vec{E}_t^{(p)} \times \vec{H}_{t,m}^{(p)}) \cdot d\vec{\Omega} & = & \tilde{a}_m^{(p)} + \tilde{b}_m^{(p)} & = & w_m^{(p)}, \\
& & & & \\
\frac{1}{\eta_m} \int_{\Omega} (\vec{E}_t^{(p+\Delta p)} \times \vec{H}_{t,m}^{(p)}) \cdot d\vec{\Omega} & = & \tilde{a}_m^{(p+\Delta p)} + \tilde{b}_m^{(p+\Delta p)} & = & w_m^{(p+\Delta p)}
\end{array}
\tag{6}
$$

with

$$
\begin{array}{llll}
\vec{E}_t^{(p)} & = & \vec{E}_t(z_p), & \vec{E}_t^{(p+\Delta p)} & = & \vec{E}_t(z_{p+\Delta p}), \\
\vec{H}_{t,m}^{(p)} & = & \vec{H}_{t,m}(z_p), & \vec{H}_{t,m}^{(p+\Delta p)} & = & \vec{H}_{t,m}(z_{p+\Delta p}).
\end{array}
\tag{7}
$$

We get $\vec{E}_t^{(p)}$ solving eigenvalue problems for the transmission lines (see section 5). $H_{t,m}^{(p)}$ can be computed from the known electric field $E_{t,m}$ of mode m (see section 8). The values of the weighted mode amplitude sums $w_m^{(p)}$ are given (see the discussion to follow). Thus, the normalization constant η_m can be computed by evaluating the orthogonality relation in the first equation of (6). $\vec{E}_t^{(p+\Delta p)}$ is computed solving a boundary value problem for the discontinuity (see section 3). Thus, the weighted mode amplitude sums $w_m^{(p+\Delta p)}$ can be calculated by using the second equation of (6).

The scattering matrix is defined with $\tilde{a}_m^{(p)}$ and $\tilde{b}_m^{(p)}$. By eliminating $\tilde{a}_m^{(p+\Delta p)}$ and $\tilde{b}_m^{(p+\Delta p)}$ in (6) we obtain

$$
\begin{aligned}
\tilde{a}_m^{(p)} &= \frac{w_m^{(p)} e^{+jk_{zm}^{(p)}\Delta z_p} - w_m^{(p+\Delta p)}}{e^{+jk_{zm}^{(p)}\Delta z_p} - e^{-jk_{zm}^{(p)}\Delta z_p}} \quad, \\[2mm]
\tilde{b}_m^{(p)} &= \frac{w_m^{(p+\Delta p)} - w_m^{(p)} e^{-jk_{zm}^{(p)}\Delta z_p}}{e^{+jk_{zm}^{(p)}\Delta z_p} - e^{-jk_{zm}^{(p)}\Delta z_p}} \quad.
\end{aligned}
\tag{8}
$$

By using (8) reflection coefficients

$$
r_m^{(p)} = \frac{\tilde{b}_m^{(p)}}{\tilde{a}_m^{(p)}} = \frac{e^{-jk_{zm}^{(p)}\Delta z_p} - \frac{w_m^{(p+\Delta p)}}{w_m^{(p)}}}{\frac{w_m^{(p+\Delta p)}}{w_m^{(p)}} - e^{+jk_{zm}^{(p)}\Delta z_p}}
\tag{9}
$$

are computed for all modes $\rho = 1(1)m_s$ and all excitations $\nu = 1(1)m_s$. The excitations are given and can be described by the vectors

$$
\vec{w}_\nu = (\bar{w}_{1,\nu}, \ldots, \bar{w}_{\rho,\nu}, \ldots, \bar{w}_{m_s,\nu})^T, \quad \nu = 1(1)m_s,
\tag{10}
$$

with, for example

$$
w_m^{(p)} = 1.0, \quad m = 1(1)m^{(p)}, \quad p = 1(1)\bar{p},
\tag{11}
$$

$$
\bar{w}_{\rho,\nu} = \begin{cases} |w_m^{(p)}| & \text{for } 1 \le \rho \le m_s + 1 - \nu \\ -|w_m^{(p)}| & \text{for } m_s + 2 - \nu \le \rho \le m_s \end{cases}, \quad \rho = m + \sum_{q=1}^{p-1} m^{(q)}.
\tag{12}
$$

This choice of $\vec{w}_\nu$ guarantees that the excitations are linearly independent. With this choice of $\bar{w}_{\rho,\nu}$ the vectors $\vec{r}_\nu$, $\vec{a}_\nu$ and $\vec{b}_\nu$ are built up analogously (see (8) and (9)):

$$
\begin{aligned}
\vec{r}_\nu &= (\bar{r}_{1,\nu}, \ldots, \bar{r}_{\rho,\nu}, \ldots \quad, \bar{r}_{m_s,\nu})^T, & \bar{r}_{\rho,\nu} &= r_m^{(p)}, \\
\vec{a}_\nu &= (\bar{a}_{1,\nu}, \ldots, \bar{a}_{\rho,\nu}, \ldots \quad, \bar{a}_{m_s,\nu})^T, & \bar{a}_{\rho,\nu} &= \tilde{a}_m^{(p)}, \\
\vec{b}_\nu &= (\bar{b}_{1,\nu}, \ldots, \bar{b}_{\rho,\nu}, \ldots \quad, \bar{b}_{m_s,\nu})^T, & \bar{b}_{\rho,\nu} &= \tilde{b}_m^{(p)}.
\end{aligned}
\tag{13}
$$

That means, we have to solve m_s boundary value problems with the boundary condition

$$
\vec{E}_{t,\nu} = \sum_{\rho=1}^{m_s} \bar{w}_{\rho,\nu} \vec{E}_{t,l}^{(p)}, \quad \rho = l + \sum_{q=1}^{p-1} m^{(q)}, \quad p = 1(1)\bar{p}, \quad \nu = 1(1)m_s,
\tag{14}
$$

in order to compute $w_m^{(p+\Delta p)}$ and $\vec{r}_\nu$.

The scattering matrix S (see (1)) is defined by

$$\vec{b}_\nu = S\vec{a}_\nu, \quad \nu = 1(1)m_s, \tag{15}$$

or (see (13))

$$\bar{b}_{\rho,\nu} = \sum_{\sigma=1}^{m_s} S_{\rho,\sigma} \cdot \bar{a}_{\sigma,\nu}, \quad \rho, \nu = 1(1)m_s. \tag{16}$$

Because of (6) and (9) we have

$$\begin{aligned}\bar{a}_{\rho,\nu}(1 + \bar{r}_{\rho,\nu}) &= \bar{w}_{\rho,\nu}, \\ \bar{b}_{\rho,\nu}(1 + \bar{r}_{\rho,\nu}) &= \bar{r}_{\rho,\nu}\bar{w}_{\rho,\nu},\end{aligned} \quad \rho, \nu = 1(1)m_s. \tag{17}$$

Multiplying Equation (16) with the product $\prod_{\mu=1}^{m_s}(1 + \bar{r}_{\mu,\nu})$ gives

$$\bar{b}_{\rho,\nu} \prod_{\mu=1}^{m_s}(1 + \bar{r}_{\mu,\nu}) = \sum_{\sigma=1}^{m_s} S_{\rho,\sigma} \bar{a}_{\sigma,\nu} \prod_{\mu=1}^{m_s}(1 + \bar{r}_{\mu,\nu}), \quad \rho, \nu = 1(1)m_s. \tag{18}$$

Substitution of (17) into the relation (18) gives

$$R_{\rho,\nu} = \sum_{\sigma=1}^{m_s} S_{\rho,\sigma} W_{\sigma,\nu} \text{ with } W_{\rho,\nu} = \bar{w}_{\rho,\nu} \prod_{\substack{\mu=1 \\ \mu \neq \rho}}^{m_s}(1 + \bar{r}_{\mu,\nu}), \ R_{\rho,\nu} = \bar{r}_{\rho,\nu} W_{\rho,\nu} \tag{19}$$

or written as matrix equation:

$$R = SW. \tag{20}$$

That means, we have to solve m_s linear algebraic equations in order to compute the $(m_s)^2$ coefficients of S:

$$W^T(S_{\rho,1}, \ldots, S_{\rho,m_s})^T = (R_{\rho,1}, \ldots, R_{\rho,m_s})^T, \quad \rho = 1(1)m_s. \tag{21}$$

3 Boundary Value Problem

A three-dimensional boundary value problem can be formulated using the integral form of Maxwell's equations in the frequency domain in order to compute the electromagnetic field:

$$\oint_{\partial\Omega} \vec{H} \cdot d\vec{s} = \int_\Omega \jmath\omega[\epsilon]\vec{E} \cdot d\vec{\Omega}, \qquad \oint_{\cup\Omega} ([\epsilon]\vec{E}) \cdot d\vec{\Omega} = 0, \tag{22}$$

$$\oint_{\partial\Omega} \vec{E} \cdot d\vec{s} = -\int_\Omega \jmath\omega[\mu]\vec{H} \cdot d\vec{\Omega}, \qquad \oint_{\cup\Omega} ([\mu]\vec{H}) \cdot d\vec{\Omega} = 0, \tag{23}$$

$$\vec{D} = [\epsilon]\vec{E}, \ \ \vec{B} = [\mu]\vec{H}, \ \ [\epsilon] = \text{diag}\,(\epsilon_x, \epsilon_y, \epsilon_z), \ \ [\mu] = \text{diag}\,(\mu_x, \mu_y, \mu_z). \tag{24}$$

Here $\vec{D}$ and $\vec{B}$ are the electric and magnetic flux density, respectively. In the left-hand sides of formulae (22) and (23) Ω is an open surface surrounded by a closed contour $\partial\Omega$, while in the right-hand sides of (22) and (23) $\cup\Omega$ is a closed surface with an interior volume. The direction of the element $d\vec{s}$ of the contour $\partial\Omega$ is such that when a right-handed screw is turned in that direction, it will advance in the direction of the vector element $d\vec{\Omega}$.

At the ports p the transverse electric field $\vec{E}_t(z_p)$ is given by superposing transmission line modes $\vec{E}_{t,l}(z_p)$ (see (14)):

$$\vec{E}_t(z_p) = \sum_{l=1}^{m^{(p)}} w_l(z_p)\vec{E}_{t,l}(z_p). \tag{25}$$

The transverse electric mode fields have to be computed solving an eigenvalue problem for the transmission lines (see section 5). All other parts of the surface of the computation domain are assumed to be an electric or a magnetic wall:

$$\vec{E} \times \vec{n} = 0 \quad \text{or} \quad \vec{H} \times \vec{n} = 0. \tag{26}$$

In order to simulate open structures, the Perfectly Matched Layer absorbing boundary condition is implemented, namely the uniaxial PML formulation according to [12]. The PML region is filled with an artificial material with complex anisotropic material properties. A complex permittivity $[\epsilon]$ and a complex permeability $[\mu]$ diagonal tensor are introduced, resulting in a reflection free interface between the computational area and the lossy PML region.

4   Grid Equations

Maxwell's equations are discretized using staggered nonequidistant rectangular grids. Using the Finite Integration Technique (FIT) [19], [1], [7] with the lowest order integration formulae

$$\oint_{\partial\Omega} \vec{f} \cdot d\vec{s} \approx \sum(\pm f_i s_i), \quad \int_{\Omega} \vec{f} \cdot d\vec{\Omega} \approx f\Omega \tag{27}$$

Equations (22), (23) are transformed into a set of grid equations:

$$A^T D_{s/\mu}\vec{b} = \jmath\omega\epsilon_0\mu_0 D_{A_\epsilon}\vec{e}, \qquad\qquad B D_{A_\epsilon}\vec{e} = 0, \tag{28}$$

$$AD_s\vec{e} = -\jmath\omega D_{A_\mu}\vec{b}, \qquad\qquad \tilde{B}D_{A_\mu}\vec{b} = 0. \tag{29}$$

The vectors $\vec{e}$ and $\vec{b}$ contain the components of the electric field intensity and the magnetic flux density of the elementary cells, respectively. The diagonal matrices $D_{s/\mu}$, D_{A_ϵ}, D_s, and D_{A_μ} contain the information on cell dimension and material. A, B, and $\tilde{B}$ are sparse.

By eliminating the components of the magnetic flux density from the two equations on the left-hand sides of (28) and (29), we get the system of linear algebraic equations

$$(A^T D_{s/\mu} D_{A_\mu}^{-1} A D_s - k_0^2 D_{A_\epsilon})\vec{e} = 0, \quad k_0 = \omega\sqrt{\epsilon_0\mu_0}, \tag{30}$$

which have to be solved using the boundary conditions (25) and (26), possibly supplemented by PML. k_0 is the wavenumber in vacuum.

5 Eigenvalue Problem

The field distribution at the ports is computed assuming longitudinal homogeneity for the transmission line structure. Thus, any field can be expanded into a sum of so-called modal fields which vary exponentially in the longitudinal direction:

$$\vec{E}(x, y, z \pm 2h) = \vec{E}(x, y, z)e^{\mp \jmath k_z 2h}. \tag{31}$$

k_z is the propagation constant. $2h$ is the length of an elementary cell in z-direction. We consider the field components in three consecutive elementary cells. The electric field components of the vector $\vec{e}$ (see (30)) $E_{x_{i,j,k+1}}$, $E_{x_{i,j,k-1}}$, $E_{y_{i,j,k+1}}$, $E_{y_{i,j,k-1}}$, $E_{z_{i,j,k-1}}$, $E_{z_{i+1,j,k-1}}$, and $E_{z_{i,j+1,k-1}}$ are expressed by the values of cell k using ansatz (31). The longitudinal electric field components E_z can be eliminated by means of the electric-field divergence equation $BD_{A_\epsilon}\vec{e} = 0$ (see (28)). Thus, we get an eigenvalue problem for the transverse electric field $\underline{e}$ on the transmission line region:

$$C\underline{\vec{e}} = \gamma\underline{\vec{e}}, \quad \gamma = e^{-\jmath k_z 2h} + e^{+\jmath k_z 2h} - 2 = -4\sin^2(hk_z). \tag{32}$$

The sparse matrix C is in general nonsymmetric complex. The order of C is $n = 2n_x n_y - n_b$. $n_x n_y$ is the number of elementary cells at the port. The size n_b depends on the number of cells with perfectly conducting material. The relation between the propagation constants k_z and the eigenvalues γ is nonlinear, and can be expressed as

$$k_z = \frac{\jmath}{2h}\ln\left(\frac{\gamma}{2} + 1 + \sqrt{\frac{\gamma}{2}\left(\frac{\gamma}{2} + 2\right)}\right) = \beta - \jmath\alpha. \tag{33}$$

We are interested only in a few modes with the smallest attenuation. These are the modes with the smallest magnitude of imaginary part, but possibly with large real part of their propagation constant. The computation of all eigenvalues in order to find a few propagation constants must be avoided for the high-dimensional problem. For numerical treatment we have to limit the search for propagation constants by setting a maximum value k_f for their real parts. A reasonable estimation of this maximum value is derived for the lossy case including PML for inhomogeneously filled waveguides in [8]:

$$\Re(k_z) \leq k_f = \omega\Re(\sqrt{\epsilon_m\mu_m}). \tag{34}$$

ϵ_m and μ_m are properties of the material that yields the largest value of the right-hand side of Equation (34). Using the limited k_f and a preset maximum value

α_m of the imaginary part of the propagation constants the region containing the interesting constants is defined as a rectangle $\hat{F}$ bounded by the lines (see Fig. 3)

$$\beta = \pm k_f \quad \text{and} \quad \alpha = \pm \alpha_m. \tag{35}$$

We can use the approximation $\sin(x) \approx x$ in (32) if we choose h to be small enough, which is necessary in any case in order to get small discretization errors:

$$\gamma = -4 \sin^2(hk_z) \approx -4(hk_z)^2 = u + jv. \tag{36}$$

With the aid of the approximation (36) the conformal mapping (33) between the plane of eigenvalues (γ-plane, see Fig. 2) and the plane of propagation constants (k_z-plane, see Fig. 3) simplifies to:

$$u = -4h^2(\beta^2 - \alpha^2), \quad v = 8h^2\alpha\beta. \tag{37}$$

Under this mapping the rectangle $\hat{F}$ of the k_z-plane is transformed into a region F of the γ-plane bounded by the two parabolas

$$v = \pm 4hk_f \sqrt{u + 4h^2k_f{}^2} \quad \text{and} \quad v = \pm 4h\alpha_m \sqrt{-u + 4h^2\alpha_m{}^2}. \tag{38}$$

This means, we have to find all eigenvalues of the region bounded by the parabolas.
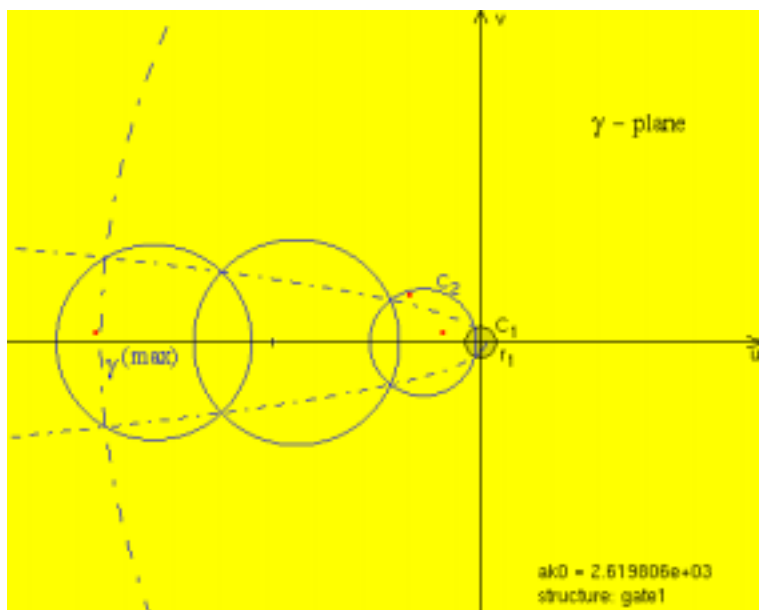
Figure 2: γ-plane

6   Computation of Eigenmodes

We need an algorithm that computes just a few selected eigenvalues and eigenvectors of a complex sparse matrix. A state-of-the-art algorithm for such problems is the
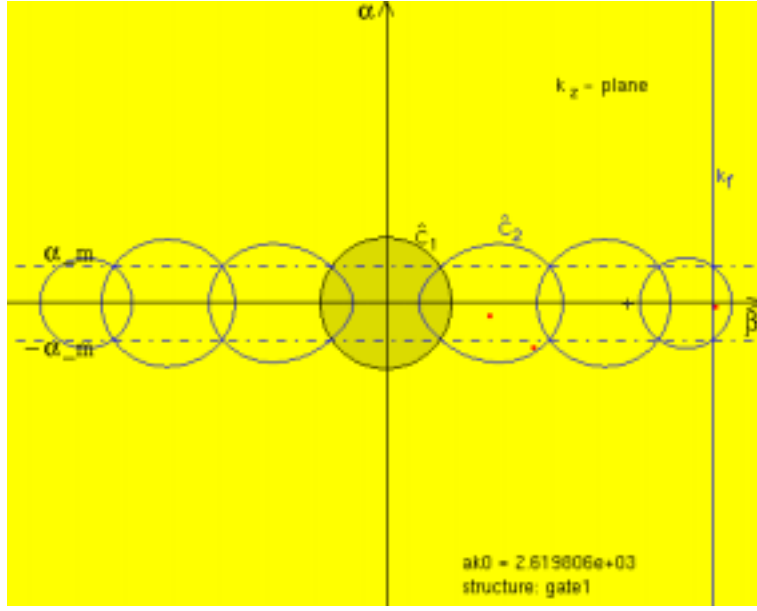
10

Figure 3: k_z-plane

Arnoldi method. In general, the Arnoldi method converges for our problem only using the invert mode and looking for eigenvalues of largest magnitude. Thus, a simple way to find the eigenvalues located in the region F would be to look for all eigenvalues of smallest magnitude, which are located in a circle centered on the origin and covering the region F. Because of the high wavenumber k_f, the number of eigenvalues located in this circle is too large in general for a feasible computation using an iterative method. We can solve this problem covering the region F with $s \geq 1$ circles C_i, $i = 1(1)s$, centered on the u-axis and calculating the eigenvalues located in these circles. That is done in the following way. First s points

$$\hat{P}_i(\beta_i, \alpha_m), \quad i = 1(1)s, \quad \beta_1 = \frac{k_f}{s} \geq \bar{\beta}, \quad \beta_s = k_f, \quad \text{with} \quad \bar{\beta} = \sqrt{3}\alpha_m \qquad (39)$$

are defined on the interval $[0, k_f]$ of the line $\alpha = \alpha_m$. The distance between the points is controlled as shown below. Even the meaning of the distance $\bar{\beta}$ is discussed below. The points $\hat{P}_i$ are transformed into the points P_i of the γ-plane. They are located on the parabola ((38), right formula). The s circles C_i of the γ-plane (see Fig. 2)

$$(u - m_i)^2 + v^2 = r_i{}^2, \quad r_i = \sqrt{(\Re(P_i) - m_i)^2 + (\Im(P_i))^2}, \quad i = 1(1)s, \qquad (40)$$

with

$$m_1 = 0, \quad m_i = \frac{(\Re(P_i))^2 - (\Re(P_{i-1}))^2 + (\Im(P_i))^2 - (\Im(P_{i-1}))^2}{2|\Re(P_i) - \Re(P_{i-1})|} \qquad (41)$$

are centered on the u-axis, covering the region bounded by the parabolas.

In order to find all eigenvalues, located in the circle C_i, l points Q_j are defined on the periphery of C_i. The matrix C is extended by the diagonal matrix Q. The

11

diagonal elements of Q are the l complex elements Q_j:

$$\bar{C} = \begin{pmatrix} Q & \\ & C \end{pmatrix}, \quad Q = diag(Q_1, ..., Q_l). \tag{42}$$

The s eigenvalue problems

$$(\bar{C} - m_i I)\vec{\underline{e}} = (\gamma - m_i)\vec{\underline{e}}, \quad i = 1(1)s, \tag{43}$$

are solved with the aid of the implicitly restarted Arnoldi method using the invert mode. The eigenvalue problems can be solved separately. The eigenvalue problems can also be computed for subintervals defined by

$$i = i_1(1)i_2 \text{ or } i = i_2(-1)i_1, \ \ 1 \leq i_1 < i_2 \leq s. \tag{44}$$

The user can profit from this property, if he knows something about the location of the interesting modes. (44) can also be used to parallelize the computation of the propagating modes (see section 10).

We consider one circle $C_i, \ i \geq 2$. The number m of eigenvalues to be computed for this circle must be l on the first call to the Arnoldi procedure. The main idea is to raise m by l until at least one value Q_j was found. But, since $m \ll \bar{n}$ ($\bar{n}$ is the order of matrix $\bar{C}$) for a feasible computation, one has to restrict the number m of required eigenvalues by m_{max}. If m exceeds m_{max}, we insert a point $\hat{P}_{i-\frac{1}{2}}$ between $\hat{P}_{i-1}$ and $\hat{P}_i$ and restart with $m = l$. The same procedure is used if a given number ν_{max} of iterations in the Arnoldi method is exceeded. We define a minimum distance between two points $\hat{P}_{i-1}$ and $\hat{P}_{i-\frac{1}{2}}$ in order to restrict the overlapping size of the circles. If the condition

$$\Delta \hat{P} = \Re(\hat{P}_{i-1}) - \Re(\hat{P}_{i-\frac{1}{2}}) \geq 2\alpha_m \tag{45}$$

cannot be fulfilled, we restart with new parameters m_{max}, ν_{max} and possibly α_m. If all eigenvalues Q_j are found in case of $m > l$, we look for the eigenvalue γ_{max} of largest magnitude. If $\sqrt{|\gamma_{max}|} > r_i$, a new circle $\tilde{C}_i$ of radius $\sqrt{|\gamma_{max}|}$ with the same center as C_i is defined. The left intersection point of this circle with the parabola ((38), right formula) is used as new point P_i, and $\Delta \hat{P} = \Re(\hat{P}_i) - \Re(\hat{P}_{i-1})$ as distance for the next step. m is reduced by the number of eigenvalues with $\sqrt{|\gamma|} > r_i$ for the next circle.

Because in general the Arnoldi method does not converge using the regular mode for our eigenvalue problem the invert mode with shifting (see (43)) is applied. A time and memory consuming system of partly ill-conditioned nonsymmetric complex linear algebraic equations has to be solved on each iteration step in this case. The linear sparse solver PARDISO [13], [14] is applied in order to fulfill the high accuracy requirements of the eigenvalue problem. The algorithm is split into three phases: symbolic factorization, numerical factorization, and forward and backward solve. The symbolic factorization can be used for all modified matrices of our problem. The

12

numerical factorization has to be repeated for every new shift. The factorization is applied to matrix C. The diagonal matrix Q (see (42)) is considered in the forward and backward solve phase.

The typical ratio of factorization time to solution time on a single CPU can be used to define ν_{max} in the subinterval control process. This ratio amounts on the average to 20 using the linear sparse solver PARDISO. That means, the costs using $\nu_{max} = 60$ Arnoldi iterations for the computation of m eigenmodes in a circle C_i defined by the points P_{i-1}, P_i are comparable with the costs, defined by the costs for two circles defined by the points $P_{i-1}, P_{i-\frac{1}{2}}$ and and $P_{i-\frac{1}{2}}, P_i$ using $\nu_{max} = 20$ iterations. On the other hand the time is lost, interrupting the computation of m eigenmodes after $\nu_{max} = 60$ iterations and starting a new iteration process for two reduced circles. Thus, we use a greater ν_{max} (see section 11 for an example). Moreover, due to the significant difference between the length and the height of the rectangular region $\hat{F}$ in the k_z-plane we have to solve a large number s of eigenvalue problems (see section 10). In order to diminish this number we use large intervals in the k_z-plane, i.e., circles with relatively large diameters in the γ-plane. That means, a number of non desired eigenvalues outside of the area F has to be calculated. In general the computation of a large number m of eigenvalues in one circle needs more iterations than a small number.

Separating the new values on each eigenvalue problem i, we are sure to have found all eigenvalues which are located in the corresponding circles C_i. Applying the mapping (37) the circles C_i (see (40)) are transformed into Cassinian curves $\hat{C}_i$ (see Fig. 3)

$$(\beta^2 + \alpha^2)^2 - \frac{m_i}{2h^2}(\beta^2 - \alpha^2) = \frac{r_i{}^2}{16h^4} - \frac{m_i{}^2}{16h^4}, \tag{46}$$

which cover the rectangle $\hat{F}$ containing all desired propagation constants. Propagation constants outside of $\hat{F}$ and PML-modes are eliminated.

The Cassinian curves $\hat{C}_i, i = 2(1)s$, consist of two disjoint ovals [3], if

$$r_i < m_i. \tag{47}$$

That means, the circles C_i may neither cut nor be tangent to the v-axis. (47) can be fulfilled by a special choice of $\hat{P}_1$:
Because of $m_1 = 0$ (see (41)) the Cassinian curve $\hat{C}_1$ (see (46)) is a circle:

$$\beta^2 + \alpha^2 = \hat{r}_1^2 = \frac{r_1}{4h^2}. \tag{48}$$

The radius r_1 of C_1 may be defined by $\hat{P}_1(\bar{\beta}, \alpha_m)$ (see (39) and (48)). A circle

$$C_2 : \quad (u + r_1)^2 + v^2 = r_1{}^2 \tag{49}$$

of radius $r_2 = r_1$ with the center $M_2(-r_1, 0)$ is evidently tangent to the v-axis. Because of (37) and (48) the point $P_1(u_1 = -\frac{r_1}{2}, v_1 = \frac{\sqrt{3}}{2}r_1)$ is an intersection point

13

of C_2 with the parabola ((38), right formula), if $\bar{\beta} = \sqrt{3}\alpha_m$. All circles C_i with a center left of M_2 and the intersection point P_1 cut the u-axis left of the v-axis. Thus, using $\bar{\beta}$ as minimum distance between the origin and $\hat{P}_1$ (see (39)) other shapes of Cassinian curves (e.g. waisted ovals, see Fig. 4 and 5), which would lead to higher execution times, are avoided.
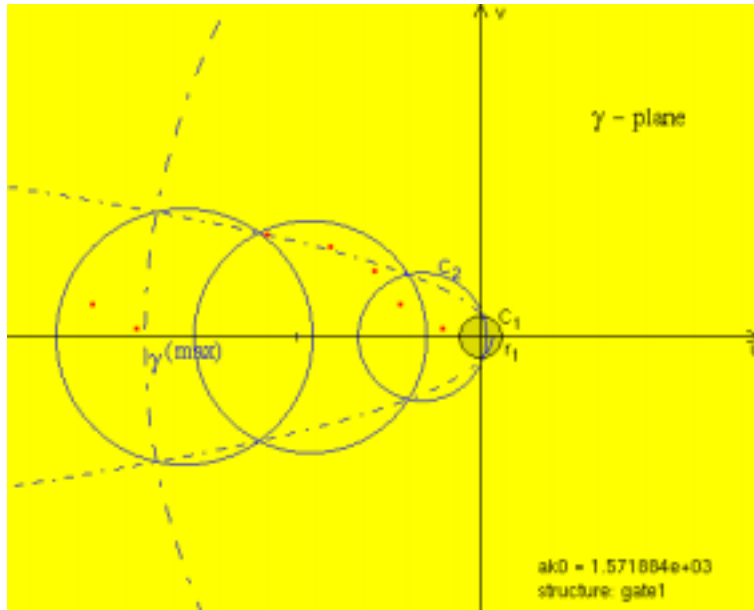

Figure 4: γ-plane, circle C_2 cut the v-axis

7   Power Part Criterion

The PML is applied in order to compute the eigen modes of open waveguide structures simulating the infinite space. Introducing the PML permits the calculation of radiation effects. Additionally the absorbing boundary suppresses the interaction between the waveguide modes and higher order modes, caused by the finite simulation domain. However, undesired so-called PML-modes are generated, due to the electric or magnetic walls behind these absorbing boundary layers, and the PML shifts only gently these box modes within the area $\hat{F}$ (see (35)). Therefore we need an additional tool to distinguish these PML-modes from the desired ones. As a result of our numerical calculations we found that examination of the eigenfunctions provides a usefull criterion to select the modes of interest. As a criterion to distinguish between waveguide modes and undesired modes we use the power concentration of all modes by way of comparison. Undesired modes are characterized by a high power concentration inside the PML region, while propagating modes are concentrated in the waveguide area. Thus, to eliminate the PML-modes we calculate the magnitude of the power flow (see section 8) of each computed mode in the PML ($P^{(P)}$), in the
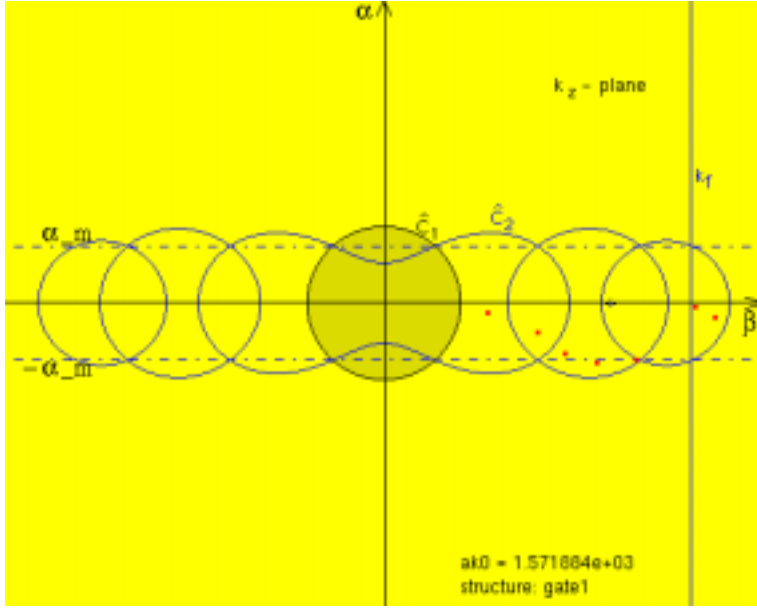
14

Figure 5: k_z-plane, waisted oval $\hat{C}_2$

waveguide region $(P^{(W)})$, and in the total computational domain (P):

$$P = P^{(P)} + P^{(W)} = \int_{\Omega^{(P)}} \left(\vec{E}_t \times \vec{H}_{t,m}^* \right) \cdot d\vec{\Omega} + \int_{\Omega^{(W)}} \left(\vec{E}_t \times \vec{H}_{t,m}^* \right) \cdot d\vec{\Omega} \,. \tag{50}$$

A mode is specified as PML-mode if the ratio

$$r^{(P)} = \frac{P^{(P)}}{P} > \xi \,, \tag{51}$$

with values $\xi = 0.2, \ldots, 0.6$, found empirically, is satisfied.

8 Computation of the Integral

We have to calculate numerically the surface integral (3) for the mode m

$$\Im = \int_{\Omega} (\vec{E}_t \times \vec{H}_{t,m}) \cdot d\vec{\Omega} = \int_{\Omega} (E_x H_{y,m} - E_y H_{x,m}) d\Omega, \tag{52}$$

in order
- to compute the electric field $E_{t,m}$ (see (6)) for the scattering matrix and
- to orthogonalize the eigenfunctions in case of multiple eigenvalues (see section 9).

Ω is the area of a port of the cross-sectional plane p. The power flux (see (50)), diverging out of a cross-sectional plane p, can be calculated in the same way, if we apply the conjugate expression $\vec{H}_{t,m}^*$ rather than $\vec{H}_{t,m}$ in (52).

15

(52) can be written as (see (24)):

$$\Im = \int_\Omega (E_x H_{y,m} - E_y H_{x,m})d\Omega = \int_\Omega (E_x[\mu]^{-1}B_{y,m} - E_y[\mu]^{-1}B_{x,m})d\Omega. \qquad (53)$$

Because the components of the electric field $\vec{E}_t$ are defined on the centers of the edges of the elementary cells and the components of the magnetic field $\vec{H}_{t,m}$ are normal to the face centers (see Fig. 6) both are located on different grid planes. Let $\overline{\Omega}$ be the grid plane which corresponds with the area Ω of a port of the cross-
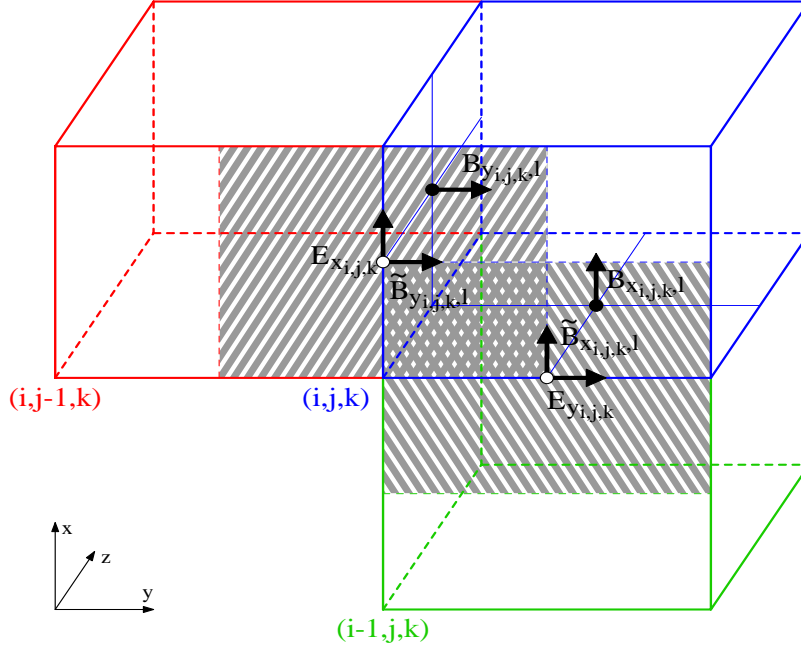
Figure 6: Integration domain

sectional plane p. Let $E_{x_{i,j,k}}$ and $E_{y_{i,j,k}}$, $i_1 \leq i \leq i_2$, $j_1 \leq j \leq j_2$, $k = const$, be the transverse electric field components on the grid plane $\overline{\Omega}$, and let $\tilde{B}_{x_{i,j,k},m}$ and $\tilde{B}_{y_{i,j,k},m}$, $i_1 \leq i \leq i_2$, $j_1 \leq j \leq j_2$, $k = const$, be the transverse magnetic flux density on the same grid plane (see Fig. 6). We use the lowest order integration formula (27) to approximate the integral (53). The material constants can be different between two different elementary cells of the primary grid. Thus, we have to divide the integration domain. The grid plane $\overline{\Omega}$ consists of $(i_2 - i_1 + 1)(j_2 - j_1 + 1)$ partial planes, and we get the following approximation of the integral:

$$\begin{aligned}
\Im = & \sum_{\substack{i_1 \leq i \leq i_2 \\ j_1 \leq j \leq j_2}} E_{x_{i,j,k}} \left(\frac{x_{i,j,k}}{2y_{i,j-1,k}} \frac{1}{\mu_{y,i,j-1,k}} \tilde{B}_{y_{i,j,k},m} + \frac{x_{i,j,k}}{2y_{i,j,k}} \frac{1}{\mu_{y,i,j,k}} \tilde{B}_{y_{i,j,k},m} \right) \\
& - \sum_{\substack{i_1 \leq i \leq i_2 \\ j_1 \leq j \leq j_2}} E_{y_{i,j,k}} \left(\frac{x_{i-1,j,k}}{2y_{i,j,k}} \frac{1}{\mu_{x,i-1,j,k}} \tilde{B}_{x_{i,j,k},m} + \frac{x_{i,j,k}}{2y_{i,j,k}} \frac{1}{\mu_{x,i,j,k}} \tilde{B}_{x_{i,j,k},m} \right)
\end{aligned} \qquad (54)$$

16

or

$$\Im = \sum_{\substack{i_1 \le i \le i_2 \\ j_1 \le j \le j_2}} E_{x_{i,j,k}} G_{x_{i,j,k},m} + \sum_{\substack{i_1 \le i \le i_2 \\ j_1 \le j \le j_2}} E_{y_{i,j,k}} G_{y_{i,j,k},m} \tag{55}$$

with

$$G_{x_{i,j,k},m} = \frac{x_{i,j,k}}{2} \Big(\frac{y_{i,j-1,k}}{\mu_{y,i,j-1,k}} + \frac{y_{i,j,k}}{\mu_{y,i,j,k}} \Big) \tilde{B}_{y_{i,j,k},m} \;, \tag{56}$$

$$G_{y_{i,j,k},m} = -\frac{y_{i,j,k}}{2} \Big(\frac{x_{i-1,j,k}}{\mu_{x,i-1,j,k}} + \frac{x_{i,j,k}}{\mu_{x,i,j,k}} \Big) \tilde{B}_{x_{i,j,k},m}$$

or

$$\Im = \vec{E}_t \cdot \vec{G}_m \quad \text{with} \quad \vec{G}_m = (\vec{G}_{x,m}, \vec{G}_{y,m})^T. \tag{57}$$

The components $G_{x_{i,j,k},m}$ and $G_{y_{i,j,k},m}$ (see (56)) contain the unknown quantities $\tilde{B}_{x_{i,j,k},m}$ and $\tilde{B}_{y_{i,j,k},m}$. They can be computed using the known electric field as follows. Because of the longitudinal homogeneity of the transmission lines we determine similar to (31)

$$B_{y_{i,j,k},m} = \tilde{B}_{y_{i,j,k},m} e^{-jk_{zm}h}, \quad B_{y_{i,j,k-1},m} = \tilde{B}_{y_{i,j,k},m} e^{+jk_{zm}h} \tag{58}$$

with

$$h = \frac{z_{i,j,k}}{2} = \frac{z_{i,j,k-1}}{2} \;. \tag{59}$$

Using this ansatz and the left-hand sides of the formulae (28) and (29) the quantities $\tilde{B}_{x_{i,j,k},m}$ and $\tilde{B}_{y_{i,j,k},m}$ can be expressed by the electric field components.

9 Orthogonalization

The orthogonality relation (3) is valid for nondegenerate modes. However, for degenerate modes we may choose a suitable linear combination of the degenerate modes such that this subset of modes is an orthogonal set. We consider the eigenvalue problem for a selected port as an example (see Fig. 7). The vector

$$\vec{a}_\kappa = \underline{\vec{e}}_l^{(\kappa)} = \underline{\vec{e}} = (\underline{\vec{e}}_x, \underline{\vec{e}}_y)^T \quad , \quad \underline{\vec{e}}_x = (\underline{e}_{x_1}, \underline{e}_{x_2}, \ldots, \underline{e}_{x_{n_{xy}}}) \quad , \quad \underline{e}_{x_\ell} = E_{x_{i,j,k}}, \\ \underline{\vec{e}}_y = (\underline{e}_{y_1}, \underline{e}_{y_2}, \ldots, \underline{e}_{y_{n_{xy}}}) \quad , \quad \underline{e}_{y_\ell} = E_{y_{i,j,k}}, \tag{60}$$

with

$$\ell = (j-1)n_x + i, \quad i = 1(1)n_x, \quad j = 1(1)n_y, \\ n_{xy} = n_x n_y, \quad \text{and} \quad k = 1 \quad \text{or} \quad k = n_z, \tag{61}$$

consists of the electric field intensity components of a port. The cross-sectional planes (see Fig. 1) can be located on the 6 different planes of the three-dimensional rectangular structure. The assumption $k = 1$ corresponds with the case, in which the cross-sectional plane (see Fig. 1) is located on the left-handed (x, y)-plane of the enclosure. We consider the boundary condition $\vec{E} \times \vec{n} = 0$ (see (26)) on the left-hand side and at the bottom of the port, that is,

$$\underline{e}_{x_\ell} = E_{x_{i,1,1}} = 0, \quad \ell = i, \quad i = 1(1)n_x, \tag{62}$$
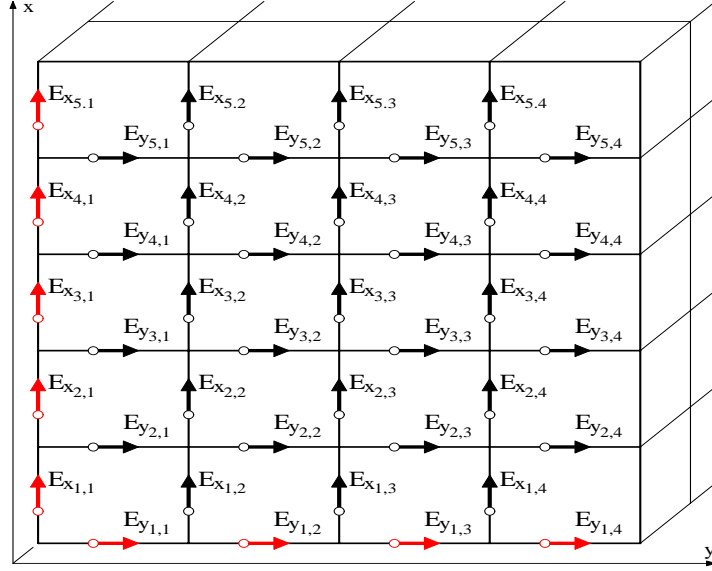
17

Figure 7: Boundary conditions on the port of the structure

and

$$\underline{e}_{y_\ell} = E_{y_{1,j,1}} = 0, \quad \ell = (j-1)n_x + 1, \quad j = 1(1)n_y. \tag{63}$$

That means, these components of the eigenvector are known, and the dimension of the eigenvalue problem (32) to be computed is reduced to

$$n = n_x n_y - n_b, \quad n_b = n_x + n_y. \tag{64}$$

Let λ_l be an eigenvalue of the matrix C (see (32) and (33)), and let ν be the algebraic multiplicity of λ_l. Then the eigenvectors $\vec{a}_\kappa = \underline{\vec{e}}_l^{(\kappa)}, \kappa = 1(1)\nu$, associated with λ_l, form a n-by-ν matrix A with $n \geq \nu$. The corresponding vectors $\vec{b}_\kappa = \underline{\vec{h}}_l^{(\kappa)}$ of the magnetic flux density components (see (65)) can be calculated as decribed in section 8.

The eigenvectors $\vec{a}_\kappa = \underline{\vec{e}}_l^{(\kappa)}, \kappa = 1(1)\nu$, generally do not fulfill the orthogonality relation (see (3), and (60) - (64))

$$\int_\Omega (\underline{\vec{e}}_l^{(\kappa_1)} \times \underline{\vec{h}}_l^{(\kappa_2)}) \cdot d\vec{\Omega} = \delta_{\kappa_1, \kappa_2}, \quad \kappa_1, \kappa_2 = 1(1)\nu, \tag{65}$$

but, the $\vec{a}_\kappa$ are linear independent. That means, that A has full column rank. Then there exists a unique n-by-ν matrix Q of vectors (modes), which fulfills the orthogonality relation (65), and an unique ν-by-ν upper triangular matrix U with positive diagonals $u_{\kappa,\kappa} > 0$ such that $A = QU$.

We can use the Gram-Schmidt algorithm [17] to orthogonalize each vector of A against the previously computed vectors according the orthogonality relation (65).

18

The Gram-Schmidt process determines the columns of Q and U recursively as follows:

We begin with

$$u_{11} = \sqrt{\int_\Omega \left(\vec{a}_1 \times \vec{b}_1\right) \cdot d\vec{\Omega}}, \quad \vec{q}_1 = \frac{\vec{a}_1}{u_{11}} \quad \text{with} \quad \vec{b}_1 = \underline{\vec{h}}_l^{(1)}. \tag{66}$$

We assume that the vectors $\vec{q}_1, ..., \vec{q}_{\kappa-1}$ of Q have been already calculated by applying the Gram-Schmidt algorithm to the linear independent vectors $\vec{a}_1, ..., \vec{a}_{\kappa-1}$ of A such that the orthogonality relation

$$\int_\Omega (\vec{q}_i \times \vec{b}_j) \cdot d\vec{\Omega} = \delta_{i,j}, \quad i, j = 1(1)\kappa - 1, \tag{67}$$

is fulfilled, and that the corresponding vectors $\vec{b}_j$ of the magnetic flux density components have been computed as described in section 8. In order to find $\vec{q}_\kappa$ with aid of $\vec{a}_\kappa$ we construct a vector

$$\vec{x} = \vec{a}_\kappa - \sum_{j=1}^{\kappa-1} u_{j,\kappa} \vec{q}_j, \tag{68}$$

which fulfills the orthogonality relation (67) for the vectors $\vec{q}_1, ..., \vec{q}_{\kappa-1}$. That gives

$$u_{j,\kappa} = \int_\Omega (\vec{q}_j \times \vec{b}_\kappa) \cdot d\vec{\Omega}, \quad j = 1(1)\kappa - 1. \tag{69}$$

We get $\vec{q}_\kappa$ by normalizing the vector $\vec{x}$ (see (67) and (68)):

$$\vec{q}_k = \vec{x}/u_{\kappa,\kappa} \tag{70}$$

with

$$u_{\kappa,\kappa} = \sqrt{\int_\Omega (\vec{x} \times \vec{b}_\kappa) \cdot d\vec{\Omega}}. \tag{71}$$

After reformulation, (68) and (70) can be written as matrix equation: $A = QU$.

10 Optoelectronic Devices

For optoelectronic devices frequencies about several hundred THz are common. The region containing potentially propagating modes grows substantially. A significant higher number of eigenvalue problems have to be solved within our algorithm. Additionally, the maximum cell size of the discretization should be less than $\frac{\lambda}{10}$, where λ denotes the wavelength in the material with the highest $\Re(\epsilon)$. Additional mesh refinements have to be used for structure regions with highly varying fields. Besides,

large cross sections are common for the waveguides under investigation. Thus, high dimensional problems have to be handled.

Due to electric and magnetic walls terminating the PML regions, undesired modes are generated inside the computation domain. These non-physical modes can be detected by examining the eigenfunctions (see section 7). Anyway, the number of eigen modes to be calculated increases because of the shifted modes.

Because of the significant difference between the magnitude of the real and imaginary part of the propagation constant a high computational accuracy is required. That means, the numerical effort increases significantly.

To overcome these problems new strategies have been realized.
The few interesting modes are located in a partial region of the longsome rectangle $\hat{F}$. By covering the corresponding area F in the plane of eigenvalues with circles (see (40) and (41)) a set of eigenpairs is scanned, which include the interesting modes. PML modes as well as propagating constants, that are located in the corresponding Cassinian curves (see (46)), but outside of $\hat{F}$, are eliminated. Additionally, the user might give an additional limit of mode numbers to be calculated. Therefore, only the remaining set of eigenpairs have to be computed with high accuracy.

Thus, to reduce the execution times, in a first step the problem is solved using a coarse grid with lower accuracy requirements in order to find approximately the locations of the interesting propagation constants. Anyway, the number of modified eigenvalue problems to be solved is high. Thus, we split the interval $[0, k_f]$ (see (39)) into subintervals (see (44)), and compute the corresponding eigenpairs independently and in parallel, for instance on different workstations or shared memory multiprocessors.

Finally the modes of interest are calculated in a second step for an essentially reduced region using a fine grid, that fulfills higher accuracy requirements. The parallel CPU mode of PARDISO provides the additional possibility to reduce the computing times for this high dimensional problem on shared memory multiprocessors without essential additional memory requirements.

11   Laser Application

As an example we have calculated the guided mode of an optoelectronic device which leads to a more moderate dimension of the corresponding eigenvalue problem. A so-called self aligned stripe (SAS) laser is investigated (see Fig. 8). The laser structure contains an additional, antiguided layer (marked with yellow color in Figure 8) outside the emitting stripe (marked with red color). This high power laser diode excites only the fundamental mode. The frequency is fixed to $300 * 10^{12}$ Hz, which corresponds to a vacuum wavelengths of 1000 nm.

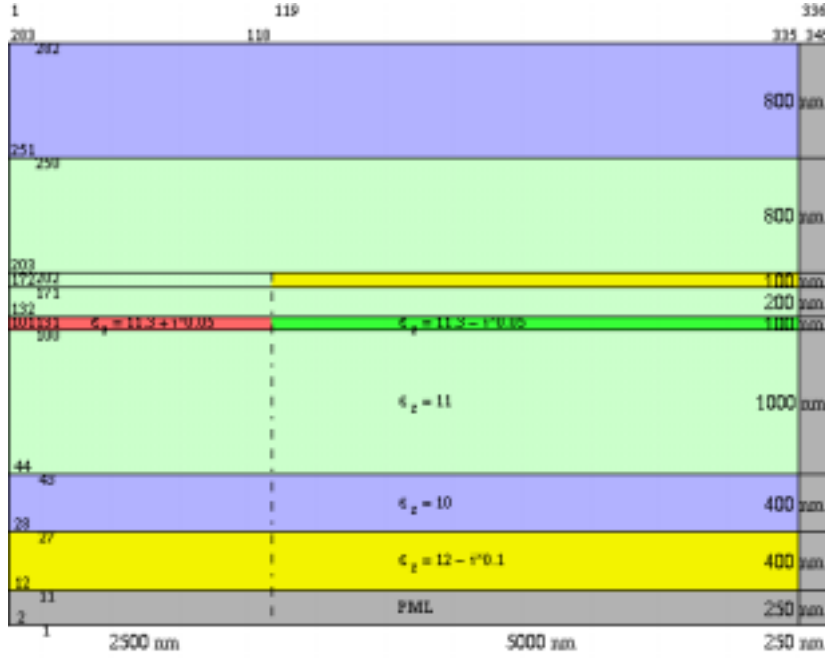A graded mesh of 121 times 127 elementary cells, including 10-cell PML regions, is

Figure 8: Laser (amplifier)

used as a coarse grid. The maximum cell size amounts 80nm, and the minimum cell size 4nm. Maximum cell size is scaled down exponentially in the vertical direction near the emitting zone and in the horizontal direction near the material cut at the end of the active zone. The dimension of the eigenvalue problem is 29 625. 84 Cassinian curves have been used to cover the long small region of the complex plane $(\alpha_m = 2500\,\mathrm{m}^{-1},\ k_f = 21\,765\,592\,\mathrm{m}^{-1},$ see (35)) containing potential guided modes. The eigenpairs have been computed with the relative accuracy $tol = 10^{-7}$, and with $m_{max} = 16,\ l = 5$ (see section 6). A maximum number $\nu_{max} = 120$ of Arnoldi iteration has been used. The total computational time amounts approximately 1 145 s. One guided mode according to the fundamental mode of the laser, was found. The circle that contains the guided mode is known after this step. The computed complex propagation constant is given by $k_z = (20\,818\,302 + j\,1\,401)\,\mathrm{m}^{-1}$ using this coarse grid.

A graded mesh of 283 times 345 elementary cells, including 10-cell PML regions, is used as a fine grid. The maximum cell size amounts $\frac{\lambda}{12} = 25$nm, where λ denotes the wavelength in the material with the highest $\Re(\epsilon)$. The minimum cell size is 1 nm. The dimension of the eigenvalue problem is 192 423. The eigenpairs have been calculated with the relative accuracy $tol = 10^{-10}$. The time to find the accurate value of the guided mode in the reduced region using the fine grid amounts only 70 s. The computed complex propagation constant is given by $k_z = (20\,817\,578 + j\,1\,488)\,\mathrm{m}^{-1}$ using the fine grid.

The calculation of all eigenvalues within the long small region $\hat{F}$ using the fine grid, needs a total computational time amount of approximately 3h and 23 minutes.

21

Thus, the computational time is reduced by a factor of 10 using a coarse and a fine grid. A Compaq Professional Workstation with processor XP1000 alpha 667 MHz has been used for the computations.

Splitting the interval $[0, k_f]$ into q subintervals (see (44)) and solving the corresponding eigenvalue problems in parallel the time for the coarse grid computation is reduced by a factor of q. Additionally, applying the parallel CPU mode of PARDISO to the fine grid computation in the reduced region the computing times for LU decomposition and for the solve phase could be reduced to 68% and 86%, respectively, using two processors.

12   System of Linear Algebraic Equations

Multiplying (30) by $D_s^{1/2}$ yields a symmetric form of linear algebraic equations:

$$\bar{A}\vec{x} = 0, \quad \bar{A} = (D_s^{1/2} A^T D_{s/\mu} D_{A_\mu}^{-1} A D_s^{1/2} - k_0^2 D_{A_\epsilon}) \tag{72}$$

with $\vec{x} = D_s^{1/2} \vec{e}$. Four kinds of preconditioning and a block quasi-minimal residual algorithm are applied to solve the large scale systems of linear algebraic equations. Details are given with [15].

The gradient of the electric field divergence (see (22), right formula)

$$[\epsilon] \nabla ([\epsilon]^{-2} \nabla \cdot [\epsilon] \vec{E}) = 0 \tag{73}$$

is equivalent to the matrix equation

$$\bar{B}\vec{x} = 0, \quad \bar{B} = D_s^{-1/2} D_{A_\epsilon} B^T D_{V_{\epsilon\epsilon}}^{-1} B D_{A_\epsilon} D_s^{-1/2}. \tag{74}$$

The diagonal matrix $D_{V_{\epsilon\epsilon}}$ is a volume matrix for the 8 partial volumes of the dual elementary cell. Taking into account the boundary conditions Equations (72) and (74) yields the form

$$\tilde{A}\vec{x} = \vec{b}, \quad \tilde{B}\vec{x} = 0. \tag{75}$$

The effect of the addition of Equations (75) can be interpreted as preconditioning with the preconditioner $(I + \tilde{B}\tilde{A}^{-1})^{-1}$ for system ((75), left equation):

$$(\tilde{A} + \tilde{B})\vec{x} = \vec{b}. \tag{76}$$

$(\tilde{A} + \tilde{B})$ is a complex indefinite symmetric matrix.

In addition, independent set orderings [11] , Jacobi and SSOR preconditioning using Eisenstat's trick [5] are applied to accelerate the speed of convergence of the used block Krylov subspace method [6] for the system of linear algebraic equations (76) that has to be solved with the same coefficient matrix, but multiple right-hand sides. The number m_s (see (2)) of right-hand sides depends on the number of ports and guided modes.

Independent set orderings are permutations P_i (see Fig. 9) to transform the matrix A_i with $A_0 = \tilde{A} + \tilde{B}$ in the form

$$A_i \quad \longrightarrow \quad P_i A_i P_i^T = \begin{pmatrix} D_i & E_i^T \\ E_i & H_i \end{pmatrix}, \tag{77}$$

where D_i is a diagonal, E_i, and H_i are sparse matrices. The unknowns of the independent set D_i are eliminated to get the next reduced matrix

$$A_{i+1} = H_i - E_i D_i^{-1} E_i^T. \tag{78}$$

We get a system of linear equations

$$P_i A_i P_i^T P_i \vec{x}_i = P_i \vec{b}_i \tag{79}$$

with $\vec{y}_i = P_i \vec{x}_i = (\vec{y}_{i,1}, \vec{y}_{i,2})^T$ and $\vec{c}_i = P_i \vec{b}_i = (\vec{c}_{i,1}, \vec{c}_{i,2})^T$ and have to solve the reduced system of linear equations

$$A_{i+1} \vec{x}_{i+1} = \vec{b}_{i+1}, \quad \vec{x}_{i+1} = \vec{y}_{i,2}, \quad \vec{b}_{i+1} = \vec{c}_{i,2} - E_i D_i^{-1} \vec{c}_{i,1} \tag{80}$$

for $\vec{y}_{i,2}$, and then we get

$$\vec{y}_{i,1} = D_i^{-1} (\vec{c}_{i,1} - E_i^T \vec{y}_{i,2}). \tag{81}$$

Then we have to permute the solution vector $\vec{y}_i$ back to the vector $\vec{x}_i$.

In comparison to the simple lossy case the number of iterations of Krylov subspace methods increases significantly in the presence of Perfectly Matched Layers (see Tab. I). The speed of convergence depends on the relations of the edges in a elementary cell of the nonequidistant rectangular grid in this case. The best results can be obtained using nearly cubic cells. Moreover, overlapping PML conditions on the corner regions of the computational domain downgrade the properties of the coefficient matrix, and should be avoided. Otherwise, eigenvalues of the matrix are shifted into the negative half plane. That means, the Krylov subspace methods need more iterations.

Acknowledgments

A_0

D_0 E_0^T E_0 H_0

D_0 E_0^T E_0 A_1

D_0 E_0^T E_0 D_1 E_1^T E_1 H_1

D_0 E_0^T E_0 D_1 E_1^T E_1 A_2

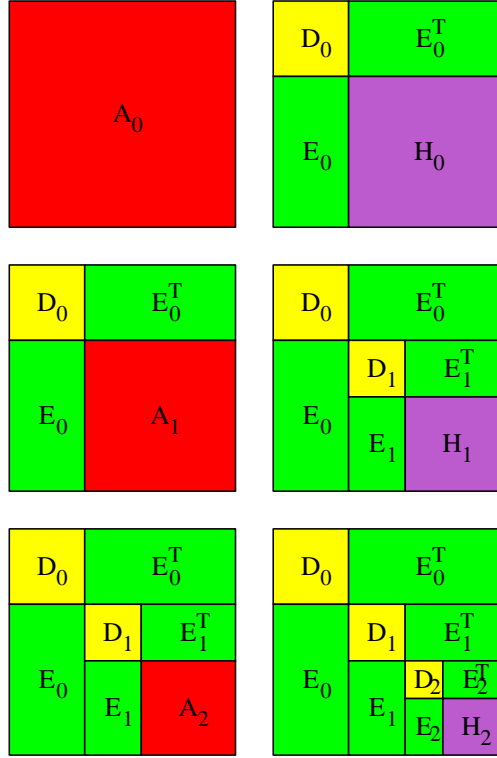D_0 E_0^T E_0 D_1 E_1^T E_1 D_2 E_2^T E_2 H_2

Figure 9: Independent set ordering

Table I: Influence of the PML setup on computational effort. The order of the system of linear algebraic equations is $40\,824$. We consider overlapping PML conditions on the corner regions.

	Number of Iterations	Number of Nonzero Elements
Structure without PML	55	235 696
Structure with PML in z-direction	489	379 220
Structure with PML in yz-direction	37 719	387 806
Structure with PML in xyz-direction	54 815	394 378
Structure with PML in xyz-direction (nonoverlapping)	458	394 378

References

[1] Beilenhoff, K., Heinrich, W., Hartnagel, H. L.: Improved Finite-Difference Formulation in Frequency Domain for Three-Dimensional Scattering Problems. IEEE Transactions on Microwave Theory and Techniques **40** (1992) 540-546

[2] Christ, A., Hartnagel, H. L.: Three-Dimensional Finite-Difference Method for the Analysis of Microwave-Device Embedding. IEEE Transactions on Microwave Theory and Techniques **35** (1987) 688–696

[3] Bronstein, I. N., Semendjajew, K.A.: Taschenbuch der Mathematik. B. G. Teubner Verlagsgesellschaft (1965)

[4] Davis, T. A., Duff, I. S.: A Combined Unifrontal/Multifrontal Method for Unsymmetric Sparse Matrices. University of Florida, Technical Report **16** (1997) 1–18

[5] Eisenstat, S. C.: Efficient implementation of a class of preconditioned conjugate gradient methods. SIAM J. Sci Statist. Comput. **2** (1981) 1–4

[6] Freund, R. W., Malhotra, W.: A Block-QMR Algorithm for Non-Hermitian Linear Systems with Multiple Right-Hand Sides. Linear Algebra and Its Applications, **254** (1997) 119–157

[7] Hebermehl, G., Schlundt, R., Zscheile, H., Heinrich W.: Improved Numerical Methods for the Simulation of Microwave Circuits, Surveys on Mathematics for Industry, **9** (1999) 117–129

[8] Hebermehl, G., Hübner, F.-K., Schlundt, R., Tischler, T., Zscheile, H., Heinrich, W.: On the Computation of Eigen Modes for Lossy Microwave Transmission Lines Including Perfectly Matched Layer Boundary Conditions. The International Journal for Computation and Mathematics in Electrical and Electronic Engineering **20** (2001) 948–964

[9] Hebermehl, G., Hübner, F.-K., Schlundt, R., Tischler, T., Zscheile, H., Heinrich, W.: Numerical Simulation of Lossy Microwave Transmission Lines Including PML. In: Scientific Computing in Electrical Engineering (ed. U. van Rienen, M. Günther, D. Hecht), Lecture Notes in Computational Science and Engineering, Springer Verlag, (2001) 267–275

[10] Lehoucq, R. B.: Analysis and Implementation of an Implicitly Restarted Arnoldi Iteration. Rice University, Department of Computational and Applied Mathematics, Technical Report **13** (1995) 1-135

[11] Saad, Y.: Iterative methods for sparse linear systems. PWS Publishing Company (1996)

[12] Sacks, Z. S., Kingsland, D. M., Lee, R., Lee, J.-F.: A Perfectly Matched Anisotropic Absorber for Use as an Absorbing Boundary Condition. IEEE Transactions on Antennas and Propagation **43** (1995) 1460–1463

[13] Schenk, O., Gärtner, K., Fichtner, W.: Efficient Sparse LU Factorization with Left-Right Looking Strategy on Shared Memory Multiprocessors. BIT **40** (2000) 158-176

[14] Schenk, O., Gärtner, K.: Two-Level Dynamic Scheduling in PARDISO: Improved Scalability on Shared Memory Multiprocessing Systems. Parallel Computing **28** (2002) 187–197

[15] Schlundt, R., Hebermehl, G., Hübner, F.-K., Heinrich, W., Zscheile, H.: Iterative Solution of Systems of Linear Equations in Microwave Circuits Using a Block Quasi-Minimal Residual Algorithm. In: Scientific Computing in Electrical Engineering (ed. U. van Rienen, M. Günther, D. Hecht), Lecture Notes in Computational Science and Engineering, Springer Verlag, (2001) 325–333

[16] Sorensen, D. C.: Implicit Application of Polynomial Filters in a k-Step Arnoldi Method. SIAM J. Matr. Anal. Apps. **13** (1992) 357–385

[17] Stoer, J., Bulirsch, R.: Introduction to Numerical Analysis, Second Edition, Springer-Verlag (1993)

[18] Tischler, T., Heinrich, W.: The Perfectly Matched Layer as Lateral Boundary in Finite-Difference Transmission-Line Analsysis. IEEE Transactions on Microwave Theory and Techniques **48** (2000) 2249-2253

[19] Weiland, T.: A Discretization Method for the Solution of Maxwell's Equations for Six-Component Fields. Electronics and Communication (AEÜ) **31** (1977) 116–120